THE JOURNAL OF PHYSICAL CHEMISTRY Letters

Letter

pubs.acs.org/JPCL

Surface Chemistry Exchange of Alloyed Germanium Nanocrystals: A Pathway Toward Conductive Group IV Nanocrystal Films

Daniel A. Ruddy,*[,†] Peter T. Erslev,[‡] Susan E. Habas,[‡] Jason A. Seabold,[†] and Nathan R. Neale*[,†]

[†]Chemical and Materials Science Center and [‡]National Center for Photovoltaics, National Renewable Energy Laboratory, 15013 Denver West Parkway, Golden, Colorado 80401, United States

Supporting Information

ABSTRACT: We present an expansion of the mixed-valence iodide reduction method for the synthesis of Ge nanocrystals (NCs) to incorporate low levels (~1 mol %) of groups III, IV, and V elements to yield main-group element-alloyed Ge NCs ($Ge_{1-x}E_x$ NCs). Nearly every main-group element (E) that surrounds Ge on the periodic table (Al, P, Ga, As, In, Sn, and Sb) may be incorporated into $Ge_{1-x}E_x$ NCs with remarkably high E incorporation into the product (>45% of E added to the reaction). Importantly, surface chemistry modification via ligand exchange allowed conductive films of $Ge_{1-x}E_x$ NCs to be prepared, which exhibit conductivities over large distances (25 μm) relevant to optoelectronic device development of group IV NC thin films.

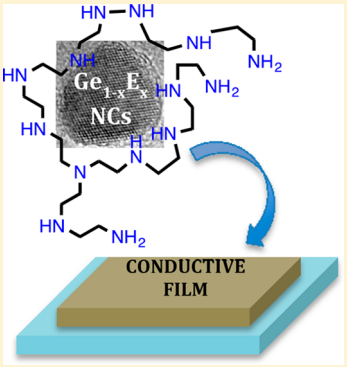

SECTION: Energy Conversion and Storage; Energy and Charge Transport

The tremendous recent progress in the methods for preparing thin films of semiconductor nanocrystals (NCs) has led to a flurry of research employing NC films as the photoactive layer in solar photoconversion,[1−3] photodetectors,[4] LEDs,[5,6] and related technologies. The majority of the research has focused on metal chalcogenide NCs, owing to the ease of performing ligand-exchange reactions at the NC surface.[7−9] These strategies have proved highly effective at displacing the long, aliphatic molecules resulting from high-temperature colloidal syntheses with small molecules that facilitate NC assembly into conductive films. In particular, recent demonstrations of NC films with mobilities as high as 1 $cm^2/V{\cdot}s$ and NC thin-film-based photovoltaic cells have been exciting for the field.[10−14]

Our group and others have been exploring methods for preparing group IV NCs, in particular, Ge NCs, as potential nontoxic infrared absorbing and emitting alternatives to metal chalcogenide or III−V quantum dots.[15−30] Group IV NCs produced from either solution approaches or vapor-phase strategies are typically functionalized via hydrosilylation (or hydrogermylation) chemistry to prepare air-stable colloidal NCs. However, the insulating alkyl surface ligands that lead to solution processability and stability also give rise to poor film conductivity, mitigating their potential usefulness in optoelectronic applications. The strong, covalently bound nature of the bonds between surface atoms and ligands results in group IV NCs that are kinetically inert to the same types of ligand-exchange reactions that can be performed on II−VI, IV−VI, and III−V NCs.

In this Letter, we report the synthesis and surface ligand-exchange chemistry of colloidally grown alloyed $Ge_{1-x}E_x$ NCs (E = main group element). We show that (1) the mixed-valence reduction method can be extended to prepare alloyed $Ge_{1-x}E_x$ NCs with extremely high incorporation efficiency of E, and (2) surface chemistry strategies can be developed to give conductive films of $Ge_{1-x}E_x$ NCs. These results suggest that further optimization of the synthesis and surface chemistry of group IV NCs could lead to device concepts with optically thick, photoactive layers.

We were initially motivated to explore alloying Ge NCs with group III, IV, and V elements that could play a role dictating n-type and p-type conductivity, as well as affecting the optical absorption, emission, and overall charge transport in NC films.[31−35] To accomplish this goal, we based our approach on our previous report of size control in the synthesis of Ge NCs prepared via the mixed-valence reduction method.[26] We found that incorporation of low levels (~1 mol %) of main group elements into Ge NCs is both possible and highly efficient via this method. In a typical synthesis (Figure 1), an oleylamine

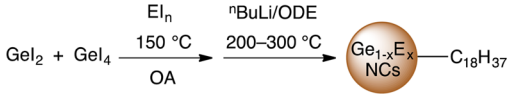

Figure 1. Reaction profile of the mixed-valence precursor reduction method for alloying main-group elements (E) into Ge NCs to yield $Ge_{1-x}E_x$ NCs (E = Al, P, Ga, Ge, As, In, Sn, and Sb).

Received: December 14, 2012
Accepted: January 11, 2013
Published: January 11, 2013

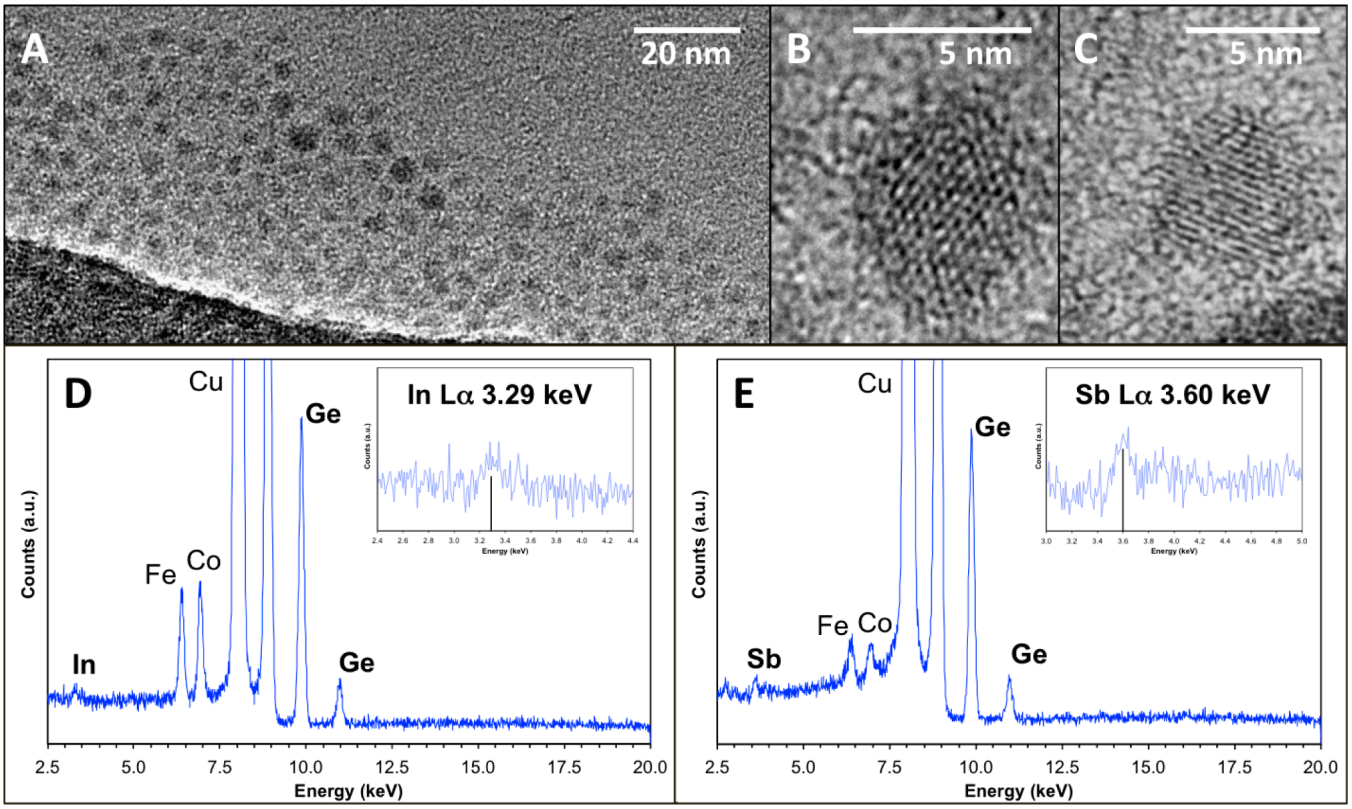

Figure 2. (A) Representative low-resolution and (B,C) high-resolution TEM images of $Ge_{1-x}E_x$ NCs. Lattice fringes in (B) and (C) correspond to the (111) plane of diamond cubic Ge with a *d*-spacing of 3.3 Å. (A,B) $Ge_{1-x}Ga_x$ NCs; (C) $Ge_{1-x}As_x$ NCs. Single-particle EDS profiles for (D) $Ge_{1-x}In_x$ NCs and (E) $Ge_{1-x}Sb_x$ NCs. The insets are expanded regions for In Lα and Sb Lα, respectively. The detection of Fe, Co, and Cu are is to the sample holder and TEM grid.

Table 1. Mol% E Incorporation Determined by ICP-OES[a] and/or XRF[b], Average NC Diameter, Absorption Onset in Tetrachloroethylene Solution, and Standard Reduction Potentials[41] of the Alloy Elements from Valence State *n*+ to 0 for the $Ge_{1-x}E_x$ NCs[c]

$Ge_{1-x}E_x$ NC	mol % E	NC diameter (nm)	abs. onset (eV)	std. red. potential (V), (*n*+)
Ge		3.8 ± 0.8	1.3	+0.247 (2+); +0.124 (4+)
$Ge_{0.991}Sn_{0.0091}$	0.91 ± 0.09[a]	3.7 ± 1.0	1.3	−0.137 (2+)
$Ge_{0.995}Al_{0.0051}$	0.51 ± 0.05[a]	3.3 ± 0.6	1.5	−1.66 (3+)
$Ge_{0.995}Ga_{0.0046}$	0.46 ± 0.05[a,b]	3.9 ± 0.9	1.3	−0.549 (3+)
$Ge_{0.989}In_{0.011}$	1.1 ± 0.1[a,b]	4.1 ± 1.0	1.2	−0.338 (3+)
$Ge_{0.989}P_{0.011}$	1.1 ± 0.1[a]	3.8 ± 0.8	1.3	−0.454 (3+)
$Ge_{0.988}As_{0.012}$	1.2 ± 0.1[a,b]	3.7 ± 0.8	1.3	+0.234 (3+)
$Ge_{0.986}Sb_{0.014}$	1.4 ± 0.2[a,b]	3.7 ± 0.8	1.3	+0.152 (3+)

[a]Determined by ICP-OES. [b]Determined by XRF. [c]Errors for multiple data points are reported as one standard deviation from the mean.

(OA) solution of a main-group element iodide (EI_n) was added to a 1:1 molar ratio solution of GeI_4 and GeI_2 in OA, and all iodide precursors were reduced with *n*-butyllithium mixed with 1-octadecene (ODE), as reported previously.[26] Representative TEM images of the resulting alloyed $Ge_{1-x}E_x$ NCs are presented in Figures 2 and S1 (Supporting Information). For all samples, the images revealed quasi-spherical particles with low aspect ratios, and high-resolution TEM imaging demonstrated single-crystal lattice fringes characteristic of diamond cubic Ge for the majority of the particles. XRD patterns with broad features are consistent with previous reports of Ge NCs from our group and others (Figure S3, Supporting Information),[23,26,36] though the peak broadness likely indicates significant amounts of incompletely crystallized (amorphous or severely strained) Ge present in the nanocrystals. This lack of crystallinity may derive from the growth mechanism, with reduction of Ge(IV) species adding amorphous or strained material to the surface of crystalline Ge cores (resulting from rapid nucleation via reduction of Ge(II) with BuLi). No other phases due to the presence of main group elements were observed (incompletely reduced EI_n, E_xO_y, α-Sn, etc.), which excludes the presence of phase segregation into large (>10 nm) crystallites that would be more easily observed by XRD. Though these XRD data do not rule out phase segregation into impurity phases, in a test case, a high concentration (10−20 mol %) of SnI_2 added to the reaction mixture was required to observe phase separation (α-Sn) in the product.

The extent to which E was incorporated into the $Ge_{1-x}E_x$ NCs was quantified via elemental analysis using inductively coupled plasma optical emission spectroscopy (ICP-OES),

dx.doi.org/10.1021/jz3020875 | J. Phys. Chem. Lett. 2013, 4, 416−421

which has been demonstrated to be an effective technique to analyze small amounts of trace elements in NCs.[31,34,37−40] Though this strategy was attempted using 1 mol % SiI_4, ICP-OES analyses for this particular element were irreproducible (showing Si in some samples but not others) and thus did not allow conclusions to be drawn about the formation of $Ge_{1-x}Si_x$ NCs. The mol % E was further corroborated for heavy elements (E = Ga, As, In, Sb) by measuring multiple areas of a drop-cast film using X-ray fluorescence (XRF) spectroscopy. The values determined using these two techniques were in good agreement (<10% deviation, Table 1). NCs incorporating the high atomic number elements In and Sb (that exhibit stronger signals than the lighter elements) were chosen for further investigation using energy-dispersive X-ray spectroscopy (EDS). To obtain adequate signal via the condensed electron beam (<50 nm in diameter), EDS was performed on both groups of several average size nanoparticles (∼4 nm in diameter) as well as on single NCs that were outside of the statistical range (∼10 nm in diameter). In both cases, the EDS results confirmed the presence of In/Sb and Ge (data for single NC EDS shown in Figure 2D, E), which indicates that the main group element is incorporated within or at the surface of the Ge NCs.

Table 1 presents the E mol % values for $Ge_{1-x}E_x$ NCs resulting from reactions employing 1 mol % E versus Ge in the solution. The high levels of incorporation efficiency (>45% relative to the amount of EI_n added to the reaction mixture) described here are extraordinary as substoichiometric incorporation is commonly observed, with only a fraction (typically less than 25%) of the element added to the reaction becoming incorporated into the product in most syntheses.[31,34,37,39,40] The simplest explanation for the differences in alloying efficiencies (particularly for Al and Ga) is that the reduction potential (Table 1) is the major determinant of growth dynamics. The full incorporation of Sn and the group V elements supports the hypothesis that the reduction potential is an important metric for precursor choice and may suggest that a critical value near −0.50 V is required for full incorporation in $Ge_{1-x}E_x$ NCs because P^{3+} (E_{red} = −0.454 V) fully incorporates whereas Ga^{3+} (E_{red} = −0.549 V) does not. Alternatively, Ge_{surf}−E or GeI_{surf}−E interactions for the Lewis acidic group III precursors may also contribute to the lower alloying efficiency of Al and Ga incorporation because E^{n+} would preferentially reside at the surface and would be less likely to become incorporated into the NC core. A related effect was recently reported in the synthesis of CdSe NCs in the presence of $InCl_3$, for which it was proposed that In^{3+} and Cl^- bind to the surface of the growing NC seed, disrupting the usual growth kinetics and resulting in wide NC size distributions.[42]

The optical absorption onsets are also presented in Table 1 and were determined from Tauc plots of the absorbance spectra (Figure S4, Supporting Information). The absorption onset values and the photoluminescence (PL, Figure S5, Supporting Information) of the $Ge_{1-x}E_x$ NCs were similar to those of the Ge NCs, exhibiting slight Stokes shifts relative to their observed band gaps determined from the Tauc plots.[26] Small deviations in observed band gaps and luminescence spectra are mostly attributable to size differences between samples (in particular, the smaller $Ge_{1-x}Al_x$ NCs). In addition, no free charge carriers were observed in NCs via optical absorption[43] nor EPR spectroscopy[44,45] as would be expected if the main-group elements acted as dopants. Thus, it appears that the extra charges from the group III and V elements are accommodated by (1) bulk and/or surface defects and/or (2) ligand bonding to surface-bound E, which results in $Ge_{1-x}E_x$ NCs that are true alloys rather than doped NCs.

The $Ge_{1-x}E_x$ NCs prepared here are passivated with insulating octadecyl surface groups ($Ge_{1-x}E_x$−$C_{18}H_{37}$), which we have found effectively shield the NCs from electrical contact. The Ge−C bond strength (255 kJ mol^{-1})[46] and covalent nature of the Ge−C bond make it kinetically stable to oxidation under ambient conditions. This beneficial surface passivation property that protects against oxidation also results in Ge−C bonds that are resistant to other chemical transformations. Thus, the ligand substitution reactions that have been used extensively in exchanging long, aliphatic ligands (trioctylphosphine, oleate, etc.) on metal chalcogenide quantum dots with small-chain molecules (ethanedithiol, hydrazine, etc.) to yield electronically coupled films[7,8] cannot be applied to $Ge_{1-x}E_x$−$C_{18}H_{37}$ NCs.

To overcome this limitation, we found that omitting ODE from the $Ge_{1-x}E_x$ NC synthesis reaction in OA results in NCs that are passivated by OA (termed $Ge_{1-x}E_x$−OA NCs) that were anticipated to be labile enough for ligand substitution reactions. Notably, Kauzlarich and co-workers recently demonstrated that OA can be used as both the reductant and the capping ligand for Ge NCs prepared using microwave heating.[47] In our synthesis, the absence of the covalent passivation by octadecyl surface groups resulted in NC aggregation with prolonged heating at 300 °C, and the synthetic procedure was modified slightly by decreasing the heating time at 300 °C to 1 min (cf. One h in the presence of ODE) and adding a small amount of OA during purification (∼0.1 mL per wash) and storage (∼1 wt % OA in hexanes). The $Ge_{1-x}E_x$−OA NC size was slightly larger than the octadecyl-capped samples, as evidenced by a slightly smaller band gap determined via a Tauc plot (∼1.05 eV for Ge−OA, cf. ∼1.20 eV for Ge−$C_{18}H_{37}$; Figure S6, Supporting Information), with the weak emission from octadecyl-capped particles completely quenched upon OA capping. The increased NC size concurs with the fact that the OA capping group is somewhat labile (vide infra), which appears to allow greater growth of the NCs during the high-temperature reduction relative to the strongly covalently bound octadecyl ligand. Similar to $Ge_{1-x}E_x$−$C_{18}H_{37}$ NC films, films drop-cast from $Ge_{1-x}E_x$−OA NCs did not exhibit conductivity, likely owing to the insulating nature of the long-chain aliphatic OA.

In an initial effort to exchange the OA ligands, drop-cast films of $Ge_{1-x}E_x$−OA NCs were immersed into solutions of various small molecules (ethylenediamine, hydrazine, methylamine, ethanedithiol, or acetic acid; 1.0 M in either ethanol or acetonitrile). FTIR spectroscopy (Figure S7, Supporting Information) of these films showed that these treatments were ineffective at removing the long OA capping group, as evidenced by little or no change in the spectra, and the resulting films remained electrically insulating, similar to the $Ge_{1-x}E_x$−$C_{18}H_{37}$ films. As an alternative to substitution with small neutral molecules, we explored treatment of $Ge_{1-x}E_x$−OA NCs with Meerwein's salt (Et_3OBF_4), which has been shown to alkylate long-chain amines and replace them with BF_4^- anions at NC surfaces, resulting in NC solubility in polar solvents such as acetonitrile.[35] The FTIR spectrum of a Ge−OA NC film soaked in 50 mM Et_3OBF_4 in acetonitrile exhibits a decrease in the alkenyl C−H stretching region near 3000 cm^{-1}, consistent with removal of some of the presumably weakly or unbound oleylamine, but the presence of C−H stretches and the absence of peaks related to surface BF_4^- ligands (expected at 1084

dx.doi.org/10.1021/jz3020875 | J. Phys. Chem. Lett. 2013, 4, 416−421

cm^{-1})[48] following treatment suggest that complete removal of oleylamine ligands was unsuccessful (Figure S6, Supporting Information).

Though ligand exchange was unsuccessful on films, amine exchange was observed during the suspension−precipitation−centrifugation procedure. Colloidal solutions of $Ge_{1-x}E_x$−OA NCs were treated with an excess of hexylamine (0.1−0.2 mL in 10 mL of toluene), and analysis of these hexylamine-capped $Ge_{1-x}E_x$ NCs using ^1H NMR spectroscopy revealed a 100-fold decrease in the OA concentration in the NCs after three solution exchanges, and a hexylamine/OA molar ratio of >1000 was determined via peak integration. However, drop-cast films prepared from hexylamine-capped $Ge_{1-x}E_x$ NCs also exhibited minimal conductivity, possibly due to the presence of trace residual OA and/or poor film quality associated with solvent and hexylamine evaporation, either of which would prevent the formation of a continuous film of close-packed NCs. Attempts to exchange NC surface ligands during the suspension−precipitation−centrifugation procedure with smaller amines, such as butylamine, ethylenediamine, or methylamine (all 0.1−0.2 mL in toluene) or with Et_3OBF_4 in biphasic hexane/acetonitrile solutions resulted in either stable suspensions from which NCs could not be precipitated or agglomeration of NCs that would not redisperse.

Another strategy for preparing continuous films of densely packed NCs in electrical contact is to use polymeric ligands. Polyethylenimine (PEI) was identified as a particularly attractive polyamine, which we hypothesized would rapidly exchange OA due to its ability to wrap the NC with multiple amine binding points and simultaneously pack NCs close together along a single chain and with as little as just one chain separating neighboring NCs (Figure 3). In addition, this

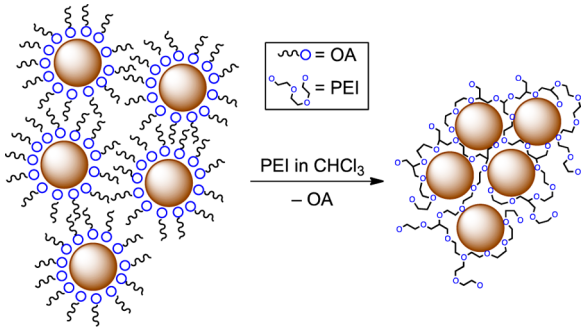

Figure 3. Surface chemistry exchange reaction of $Ge_{1-x}E_x$−OA NCs with polyethyleneimine (PEI), producing polymer-encapsulated NCs, $Ge_{1-x}E_x$−PEI NCs.

polymer has been used to form high-quality films from simple processing techniques, such as drop-casting or dip-coating.[49,50] Indeed, treatment of $Ge_{1-x}E_x$−OA NCs with a 1.7 wt % (0.25 g in 10 mL) chloroform solution of PEI immediately following purification resulted in ligand exchange, as evidenced by a change in solubility of the dark-brown product from aliphatic solvents (e.g., hexanes, toluene) with OA or octadecyl capping to polar solvents (e.g., $CHCl_3$, MeOH), consistent with the solubility properties of the parent PEI polymer. For example, after addition of hexanes to a chloroform solution of $Ge_{1-x}E_x$−PEI NCs (3:1 v/v hexanes/chloroform), the polymer-encapsulated NCs easily precipitate upon centrifugation to form a dense, dark-colored NC−polymer composite. To confirm the displacement of OA, ^1H NMR spectroscopy was employed, and the spectrum of the $Ge_{1-x}E_x$−PEI NCs did not exhibit any of the characteristic peaks for OA (in particular, the well-resolved alkenyl protons at δ = 5.4). The optical properties of the PEI-capped particles were similar to that of the parent OA-capped species (slightly reduced band gaps relative to octadecyl-capped NCs (Figure S6, Supporting Information) and no emission).

Most importantly, drop-cast films prepared with $Ge_{1-x}E_x$−PEI NCs were electrically conductive as determined by current−voltage measurements using a coplanar electrode geometry with a spacing of 25 μm (Figure 4). Consistent

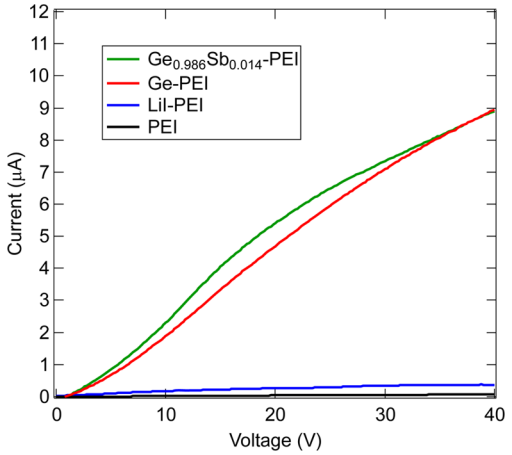

Figure 4. Representative current−voltage curves of $Ge_{1-x}E_x$−PEI NC, PEI−LiI, and PEI films prepared by drop-casting chloroform solutions onto Si/SiO_2 substrates patterned with gold contacts (2 mm length, 25 μm spacing). Data were recorded at 100 °C under an inert atmosphere.

with the optical experiments, no statistical differences were observed between the conductivities of the alloyed $Ge_{1-x}E_x$−PEI and Ge−PEI NC samples, again confirming the alloyed rather than doped nature of these species. Though currents varied from 3 to 12 μA at 40 V applied bias for all $Ge_{1-x}E_x$−PEI samples, control experiments with only PEI films (no $Ge_{1-x}E_x$ NCs) consistently demonstrated current values 1−2 orders of magnitude lower at the same applied bias. Similarly, control experiments with 50 mg of LiI (a potential contaminant resulting from the synthesis) in 250 mg of PEI showed currents at least an order of magnitude lower than those of $Ge_{1-x}E_x$−PEI films (Figure 4). These experiments suggest that electrical transport observed in the $Ge_{1-x}E_x$−PEI NCs occurs through the $Ge_{1-x}E_x$ NC network, with conductivities on the order of 10^{-3} $S{\cdot}cm^{-1}$ (calculated from the volume between the two contacts of 2 mm × 25 μm × 40 nm and average current values of 5 μA at ~20 V, where the current is linear). Notably, this calculation assumes current only flows though the $Ge_{1-x}E_x$ NC network between the two electrodes with no spreading above the 40 nm electrode height, and therefore, this value represents a lower limit to the conductivity. Several reports have achieved group IV NC conductivity as a thin film (0.1−1 μm thick) when blended with a conducting organic matrix[6,51,52] or as a very thin (30 nm) NC layer sandwiched between organic conductors.[53] In one of these reports,[52] surfactant-free Si NCs were found to exhibit ohmic behavior (at V = 0, I_{sc} = 0) in the absence of the conducting matrix, consistent with the ohmic behavior in Figure 4. Still, in these examples, photogenerated charge conduction through the NCs themselves over even

dx.doi.org/10.1021/jz3020875 | J. Phys. Chem. Lett. 2013, 4, 416−421

relatively short (>100 nm) distances was avoided, presumably owing to the limited conductivity through the NCs in these systems. Finally, Korgel and co-workers recently have shown that thermally stable Si NC superlattices can be constructed exhibiting oriented superlattice grains, but no electrical characterization was reported.[54] The demonstration here of long-range charge transport (25 μm) establishes that group IV NC superlattices can be designed for optoelectronic applications provided the appropriate NC surface chemistry or matrix is developed to facilitate charge transport.

In conclusion, expansion of the mixed-valence precursor reduction method to include low-level incorporation of main-group elements resulted in successful alloying to prepare $Ge_{1-x}E_x$ NCs. The high atom incorporation efficiency (>45%) is remarkable and represents a major synthetic advancement in synthetic methodology. Finally, surface chemistry modification by omitting ODE in the reaction mixture provided oleylamine-capped $Ge_{1-x}E_x$ NCs. Whereas a variety of small molecules were ineffective at displacing OA in Ge NCs as either colloids or in drop-cast films, the OA ligands could be substituted in solution using terminal amines such as hexylamine or polyamines such as PEI. The use of PEI allowed $Ge_{1-x}E_x$–PEI NC films to become electrically conductive, with evidence for transport occurring through the $Ge_{1-x}E_x$ NC network.

■ ASSOCIATED CONTENT

Supporting Information

Experimental protocols, representative TEM images and size histograms for all $Ge_{1-x}E_x$ NCs, X-ray diffraction patterns for $Ge_{1-x}E_x$ NCs, Tauc plots and PL spectra for $Ge_{1-x}E_x$–$C_{18}H_{37}$ NC solutions, Tauc plots for Ge–OA and $Ge_{1-x}E_x$–PEI NC solutions, and FTIR spectra of $Ge_{1-x}E_x$–OA NC films treated with various small molecules. This material is available free of charge via the Internet at http://pubs.acs.org.

■ AUTHOR INFORMATION

Corresponding Author

*E-mail: Dan.Ruddy@nrel.gov (D.A.R.); Nathan.Neale@nrel.gov(N.R.N.).

Notes

The authors declare no competing financial interest.

■ ACKNOWLEDGMENTS

The authors thank A. G. Norman (NREL) for HRTEM analysis and Lynn Gedvilas (NREL) for FTIR analysis of the $Ge_{1-x}E_x$ NCs described in this manuscript. The authors gratefully acknowledge funding for this work by the Division of Chemical Sciences, Geosciences, and Biosciences in the Office of Basic Energy Sciences of the U.S. Department of Energy under Contract No. DE-AC36-08GO28308.

■ REFERENCES

(1) Hillhouse, H. W.; Beard, M. C. Solar Cells from Colloidal Nanocrystals: Fundamentals, Materials, Devices, and Economics. *Curr. Opin. Colloid Interface Sci.* **2009**, *14*, 245–259.

(2) Nozik, A. J.; Beard, M. C.; Luther, J. M.; Law, M.; Ellingson, R. J.; Johnson, J. C. Semiconductor Quantum Dots and Quantum Dot Arrays and Applications of Multiple Exciton Generation to Third-Generation Photovoltaic Solar Cells. *Chem. Rev.* **2010**, *110*, 6873–6890.

(3) Beard, M. B. Multiple Exciton Generation in Semiconductor Quantum Dots. *J. Phys. Chem. Lett.* **2011**, *2*, 1282–1288.

(4) Konstantatos, G.; Sargent, E. H. Nanostructured Materials for Photon Detection. *Nat. Nanotechnol.* **2010**, *5*, 391–400.

(5) Wood, V.; Bulovíc, V. Colloidal Quantum Dot Light-Emitting Devices. *Nano Rev.* **2010**, *1*, 5202.

(6) Cheng, K.-Y.; Anthony, R.; Kortshagen, U. R.; Holmes, R. J. High-Efficiency Silicon Nanocrystal Light-Emitting Devices. *Nano Lett.* **2011**, *11*, 1952–1956.

(7) Luther, J. M.; Law, M.; Song, Q.; Perkins, C. L.; Beard, M. C.; Nozik, A. J. Structural, Optical, and Electrical Properties of Self-Assembled Films of PbSe Nanocrystals Treated with 1,2-Ethanedithiol. *ACS Nano* **2008**, *2*, 271–280.

(8) Law, M.; Luther, J. M.; Song, Q.; Hughes, B. K.; Perkins, C. L.; Nozik, A. J. Structural, Optical, and Electrical Properties of PbSe Nanocrystal Solids Treated Thermally or with Simple Amines. *J. Am. Chem. Soc.* **2008**, *130*, 5974–5984.

(9) Kovalenko, M. V.; Scheele, M.; Talapin, D. V. Colloidal Nanocrystals with Molecular Metal Chalcogenide Surface Ligands. *Science* **2009**, *324*, 1417–1420.

(10) Liu, Y.; Gibbs, M.; Perkins, C. L.; Tolentino, J.; Zarghami, M. H.; Bustamante, J. J.; Law, M. Robust, Functional Nanocrystal Solids by Infilling with Atomic Layer Deposition. *Nano Lett.* **2011**, *22*, 5349–5355.

(11) Luther, J. M.; Gao, J.; Lloyd, M.; Semonin, O. E.; Beard, M. C.; Nozik, A. J. Stability Assessment on a 3% Bilayer PbS/ZnO Quantum Dot Heterojunction Solar Cell. *Adv. Mater.* **2010**, *22*, 3704–3707.

(12) Semonin, O. E.; Luther, J. M.; Choi, S.; Chen, H. Y.; Gao, J. B.; Nozik, A. J.; Beard, M. C. Peak External Photocurrent Quantum Efficiency Exceeding 100% via MEG in a Quantum Dot Solar Cell. *Science* **2011**, *334*, 1530–1533.

(13) Ning, Z.; Ren, Y.; Hoogland, S.; Voznyy, O.; Levina, L.; Stadler, P.; Lan, X.; Zhitomirsky, D.; Sargent, E. H. All-Inorganic Colloidal Quantum Dot Photovoltaics Employing Solution-Phase Halide Passivation. *Adv. Mater.* **2012**, *24*, 6295–6299.

(14) Liu, H.; Zhitomirsky, S.; Hoogland, J.; Tang, I.; Kramer, J.; Ning, Z.; Sargent, E. H. Systematic Optimization of Quantum Junction Colloidal Quantum Dot Solar Cells. *Appl. Phys. Lett.* **2012**, *101*, 151112.

(15) Wilcoxon, J. P.; Provencio, P. P.; Samara, G. A. Synthesis and Optical Properties of Colloidal Germanium Nanocrystals. *Phys. Rev. B* **2001**, *64*, 035417.

(16) Gerung, H.; Bunge, S. D.; Boyle, T. J.; Brinker, C. J.; Han, S. M. Anhydrous Solution Synthesis of Germanium Nanocrystals from the Germanium(II) Precursor $Ge[N(SiMe_3)_2]_2$. *Chem. Commun.* **2005**, 1914–1916.

(17) Wang, W. Z.; Poudel, B.; Huang, J. Y.; Wang, D. Z.; Kunwar, S.; Ren, Z. F. Synthesis of Gram-Scale Germanium Nanocrystals by a Low-Temperature Inverse Micelle Solvothermal Route. *Nanotechnology* **2005**, *16*, 1126–1129.

(18) Lu, X. M.; Korgel, B. A.; Johnston, K. P. High Yield of Germanium Nanocrystals Synthesized from Germanium Diiodide in Solution. *Chem. Mater.* **2005**, *17*, 6479–6485.

(19) Ma, X. C.; Wu, F. Y.; Kauzlarich, S. M. Alkyl-Terminated Crystalline Ge Nanoparticles Prepared from NaGe: Synthesis, Functionalization and Optical Properties. *J. Solid State Chem.* **2008**, *181*, 1628–1633.

(20) Chou, N. H.; Oyler, K. D.; Motl, N. E.; Schaak, R. E. Colloidal Synthesis of Germanium Nanocrystals Using Room-Temperature Benchtop Chemistry. *Chem. Mater.* **2009**, *21*, 4105–4107.

(21) Lee, D. C.; Pietryga, J. M.; Robel, I.; Werder, D. J.; Schaller, R. D.; Klimov, V. I. Colloidal Synthesis of Infrared-Emitting Germanium Nanocrystals. *J. Am. Chem. Soc.* **2009**, *131*, 3436–3437.

(22) Kortshagen, U. Nonthermal Plasma Synthesis of Semiconductor Nanocrystals. *J. Phys. D.: Appl. Phys.* **2009**, *42*, 113001.

(23) Vaughn, D. D., II; Bondi, J. F.; Schaak, R. E. Colloidal Synthesis of Air-Stable Crystalline Germanium Nanoparticles with Tunable Sizes and Shapes. *Chem. Mater.* **2010**, *22*, 6103–6108.

(24) Henderson, E. J.; Seino, M.; Puzzo, D. P.; Ozin, G. A. Colloidally Stable Germanium Nanocrystals for Photonic Applications. *ACS Nano* **2010**, *4*, 7683–7691.

(25) Kelly, J. A.; Henderson, E. J.; Veinot, J. G. C. Sol−Gel Precursors for Group 14 Nanocrystals. *Chem. Commun.* **2010**, 8704−8718.
(26) Ruddy, D. A.; Johnson, J. C.; Smith, E. R.; Neale, N. R. Size and Bandgap Control in the Solution-Phase Synthesis of Near-Infrared-Emitting Germanium Nanocrystals. *ACS Nano* **2010**, *4*, 7459−7466.
(27) Erogbogbo, F.; Liu, T. H.; Ramadurai, N.; Tuccarione, P.; Lai, L.; Swihart, M. T.; Prasad, P. N. Creating Ligand-Free Silicon Germanium Alloy Nanocrystal Inks. *ACS Nano* **2011**, *5*, 7950−7959.
(28) Hessel, C. M.; Henderson, E. J.; Veinot, J. G. C. Hydrogen Silsesquioxane: A Molecular Precursor for Nanocrystalline Si−SiO_2 Composites and Freestanding Hydride-Surface-Terminated Silicon Nanoparticles. *Chem. Mater.* **2006**, *18*, 6139−6146.
(29) Henderson, E. J.; Kelly, J. A.; Veinot, J. G. C. Influence of $HSiO_{1.5}$ Sol−Gel Polymer Structure and Composition on the Size and Luminescent Properties of Silicon Nanocrystals. *Chem. Mater.* **2009**, *21*, 5426−5434.
(30) Mastronardi, M. L.; Maier-Flaig, F.; Faulkner, D.; Henderson, E. J.; Kübel, C.; Lemmer, U.; Ozin, G. A. Size-Dependent Absolute Quantum Yields for Size-Separated Colloidally-Stable Silicon Nanocrystals. *Nano Lett.* **2012**, *12*, 337−342.
(31) Erwin, S. C.; Zu, L. J.; Haftel, M. I.; Efros, A. L.; Kennedy, T. A.; Norris, D. J. Doping Semiconductor Nanocrystals. *Nature* **2005**, *436*, 91−94.
(32) Norris, D. J.; Efros, A. L.; Erwin, S. C. Doped Nanocrystals. *Science* **2008**, *319*, 1776−1779.
(33) Chen, D. A.; Viswanatha, R.; Ong, G. L.; Xie, R. G.; Balasubramaninan, M.; Peng, X. G. Temperature Dependence of "Elementary Processes" in Doping Semiconductor Nanocrystals. *J. Am. Chem. Soc.* **2009**, *131*, 9333−9339.
(34) Mocatta, D.; Cohen, G.; Schattner, J.; Millo, O.; Rabani, E.; Banin, U. Heavily Doped Semiconductor Nanocrystal Quantum Dots. *Science* **2011**, *332*, 77−81.
(35) Cao, Y. C. Impurities Enhance Semiconductor Nanocrystal Performance. *Science* **2011**, *332*, 48−49.
(36) Gerung, H.; Zhao, Y.; Wang, L.; Jain, R. K.; Boyle, T. J.; Brinker, C. J.; Han, S. M. Two-Photon Absorption of Matrix-Free Ge Nanocrystals. *Appl. Phys. Lett.* **2006**, *89*, 111107.
(37) Buonsanti, R.; Llordes, A.; Aloni, S.; Helms, B. A.; Milliron, D. J. Tunable Infrared Absorption and Visible Transparency of Colloidal Aluminum-Doped Zinc Oxide Nanocrystals. *Nano Lett.* **2011**, *11*, 4706−4710.
(38) Pi, X. D.; Gresback, R.; Liptak, R. W.; Campbell, S. A.; Kortshagen, U. Doping Efficiency, Dopant Location, and Oxidation of Si Nanocrystals. *Appl. Phys. Lett.* **2008**, *92*, 123102.
(39) Baldwin, R. K.; Zou, J.; Pettigrew, K. A.; Yeagle, G. J.; Britt, R. D.; Kauzlarich, S. M. The Preparation of a Phosphorus Doped Silicon Film from Phosphorus Containing Silicon Nanoparticles. *Chem. Commun.* **2006**, 658−660.
(40) Zhang, X.; Brynda, M.; Britt, R. D.; Carroll, E. C.; Larsen, D. S.; Louie, A. Y.; Kauzlarich, S. M. Synthesis and Characterization of Manganese-Doped Silicon Nanoparticles: Bifunctional Paramagnetic-Optical Nanomaterial. *J. Am. Chem. Soc.* **2007**, *129*, 10668−10669.
(41) *CRC Handbook of Chemistry and Physics*; 77th ed.; CRC Press: Boca Raton, FL, 1996−1997.
(42) Tuinenga, C.; Jasinski, J.; Iwamoto, T.; Chikan, V. *In Situ* Observation of Heterogeneous Growth of CdSe Quantum Dots: Effect of Indium Doping on the Growth Kinetics. *ACS Nano* **2008**, *2*, 1411−1421.
(43) Luther, J. M.; Jain, P. K.; Ewers, T.; Alivisatos, A. P. Localized Surface Plasmon Resonances Arising from Free Carriers in Doped Quantum Dots. *Nat. Mater.* **2011**, *10*, 368−371.
(44) Ochsenbein, S. T.; Feng, Y.; Whitaker, K. M.; Badaeva, E.; Liu, W. K.; Li, X.; Gamelin, D. R. Charge-Controlled Magnetism in Colloidal Doped Semiconductor Nanocrystals. *Nat. Nanotechnol.* **2009**, *4*, 681−687.
(45) Cohn, A. W.; Kittilstved, K. R.; Gamelin, D. R. Tuning the Potentials of "Extra" Electrons in Colloidal n-Type ZnO Nanocrystals via Mg^{2+} Substitution. *J. Am. Chem. Soc.* **2012**, *134*, 7937−7943.
(46) Buriak, J. M. Organometallic Chemistry on Silicon and Germanium Surfaces. *Chem. Rev.* **2002**, *102*, 1271−1308.
(47) Muthuswamy, E.; Iskander, A. S.; Amador, M. M.; Kauzlarich, S. M. Facile Synthesis of Germanium Nanoparticles with Size Control: Microwave versus Conventional Heating. *Chem. Mater.* **2012**, DOI: 10.1021/cm302229b.
(48) Dong, A.; Ye, X. C.; Chen, J.; Kang, Y.; Gordon, T.; Kikkawa, J. M.; Murray, C. B. A Generalized Ligand-Exchange Strategy Enabling Sequential Surface Functionalization of Colloidal Nanocrystals. *J. Am. Chem. Soc.* **2011**, *133*, 998−1006.
(49) Sun, S.; Anders, S.; Thomson, T.; Baglin, J. E. E.; Toney, M. F.; Hamann, H. F.; Murray, C. B.; Terris, B. D. Controlled Synthesis and Assembly of FePt Nanoparticles. *J. Phys. Chem. B.* **2003**, *107*, 5419−5425.
(50) Burrell, A. K.; McCleskey, T. M.; Jia, Q. X. Polymer Assisted Deposition. *Chem. Commun.* **2008**, 1271−1277.
(51) Liu, C.-Y.; Holman, Z. C.; Kortshagen, U. R. Hybrid Solar Cells from P3HT and Silicon Nanocrystals. *Nano Lett.* **2009**, *9*, 449−452.
(52) Švrček, V.; Cook, S.; Kazaoui, S.; Kondo, M. Silicon Nanocrystals and Semiconducting Single-Walled Carbon Nanotubes Applied to Photovoltaic Cells. *J. Phys. Chem. Lett.* **2011**, *2*, 1646−1650.
(53) Puzzo, D. P.; Henderson, E. J.; Helander, M. G.; Wang, Z. B.; Ozin, G. A.; Lu, Z. Visible Colloidal Nanocrystal Silicon Light-Emitting Diode. *Nano Lett.* **2011**, *11*, 1585−1590.
(54) Yu, Y.; Bosoy, C. A.; Hessel, C. M.; Smilgies, D.-M.; Korgel, B. A. Silicon Nanocrystal Superlattices. *Chem. Phys. Chem.* **2013**, *14*, 84−87.